Kinetics and mechanism for transparent polyethylene-TiO$_2$ films mediated self-cleaning leading to MB dye discoloration under sunlight irradiation

S. Rtimi [a], C. Pulgarin [a,**], R. Sanjines [b], J. Kiwi [c,*]

[a] Ecole Polytechnique Fédérale de Lausanne, EPFL-SB-ISIC-GPAO, Station 6, CH-1015, Lausanne, Switzerland
[b] Ecole Polytechnique Fédérale de Lausanne, EPFL-SB-IPMC-LNNME, Bat PH, Station 3, CH-1015, Lausanne, Switzerland
[c] Ecole Polytechnique Fédérale de Lausanne, EPFL-SB-ISIC-LPI, Bat Chimie, Station 6, CH-1015, Lausanne, Switzerland

ABSTRACT

Polyethylene-TiO$_2$ (from now on PE-TiO$_2$) transparent, non-scattering sputtered films have been found effective in the discoloration of methylene blue (MB) under low intensity solar simulated light. By Fourier transform attenuated infrared spectroscopy (ATR-FTIR), the systematic shift and decrease in the ν_s(CH$_2$) and ν_s(C=C) vibration-rotational bands was observed preceding MB discoloration. RF-pretreatment allowed a significant increase in the TiO$_2$ loading on PE compared to non-pretreated PE as shown by X-ray fluorescence (XRF). The PE-TiO$_2$ photo-switching from a hydrophobic to a hydrophilic surface was observed within 60 min under light while the reverse process was complete within 24 h in the dark. The position of the MB* and MB*/MB$^+$ levels allowing electron injecting into the TiO$_2$cb is discussed. The probability for the MB^T deactivation and of MB* reacting with O$_2$ leading to the short lived MB$^+$ cation is estimated. A mechanism for MB discoloration on PE-TiO$_2$ is suggested.

© 2014 Elsevier B.V. All rights reserved.

1. Introduction

With increasing demand for hygienic, self-disinfecting and contamination free surfaces, interest in developing self-cleaning surfaces has grown rapidly in recent times [1,2]. The photocatalytic induced self-cleaning of textiles was recently reported by Kiwi [3–8], Daoud [9,10], Radetic [11] and Pakkanen [12]. TiO$_2$ is the standard photocatalyst used in the field of environmental photochemistry. TiO$_2$ is the photocatalyst of choice for a variety of applications. Its action involves mild surface reactions using sunlight, O$_2$ (air) and water vapor (air) to produce highly oxidative radicals able to destroy organic compounds. Polyethylene (PE) used as the substrate to sputter TiO$_2$ presents thermal resistance up to 110–120 °C for short periods. The deposition/adhesion of TiO$_2$ colloids/powders on low heat resistance substrates like PE can be easily wiped out by finger or cloth. Depositions from colloids are not mechanically stable or commercial feasible [13]. The uneven distribution of colloidal TiO$_2$ layers on polymers proceeds with

low adherence and this problem is addressed in the present study depositing TiO$_2$ by sputtering [1–4].

Two routes have been suggested lately to increase the adherence and uniformity of TiO$_2$ layers on textiles, glass and polymer surfaces: (a) RF-plasma or UVC pretreatment of C-containing surfaces leading to negative charged carboxylic, or peroxo-surface functional groups in the presence of O$_2$. These negative surface groups have been shown to bind the positive TiO$_2$ on PE [4,7,8,14–16], (b) sputtering from a Ti-target in a magnetron chamber in a reactive O$_2$ atmosphere either by direct current or pulsed mode [17–21], at temperatures ≤110–120 °C. These temperatures are below the flow point of PE. TiO$_2$ photocatalysis has been extensively studied by A. Mills in relation to MB discoloration [22–25].

The photobleaching mechanism of MB sensitized on TiO$_2$ suspensions/colloids in aqueous solution is still controversial. Herrmann [26] has recently reported the degradation pathway and intermediates of MB in colloidal solutions under light. These studies take advantage of the fact that TiO$_2$ presents dense surface TiOH groups, high crystallinity and redox properties generating highly oxidative radicals and surface area leading to an effective charge carrier dynamics under light irradiation [1,13,21].

Self-cleaning surfaces are labor and energy saving materials. Further work to improve the performance of self-cleaning surfaces where the TiO$_2$ layers do not disrupt the PE-network is warranted

[1,2,13]. This study presents innovative uniform transparent PE-TiO$_2$ leading to MB discoloration focusing on: (a) MB discoloration kinetics, (b) characterization of the transparent, non scattering PE-TiO$_2$ films showing a high degree of light penetration, (c) the significant effect of the RF and UVC pretreatment of PE increasing the loading of TiO$_2$ on PE necessary to obtain sorter MB discoloration time and (d) the evidence for the stretching vibration shift of the MB–CH$_2$ groups leading to bond scission preceding MB discoloration.

2. Experimental

2.1. Pretreatment by RF-plasma and by UVC

The low-density polyethylene (LDPE) is a highly branched low crystalline film with formula H(CH$_2$–CH$_2$)$_n$H. The (LDPE) 0.1 mm thick was obtained from Longfellow (ET3112019), had a density of 0.92 g/cm^3, has an upper working temperature of 90 °C and a flowing point of 185 °C. The PE fabrics were pretreated in the cavity in air at atmospheric pressure and at 1 Torr by means of an RF-plasma unit (Harrick Corp. 13.56 MHz, 100 W) for different times. This induced functional C-chelating surface groups by the reaction of activated gas O-species with the PE surface [4,7,16]. The PE was also functionalized in air at atmospheric pressure and at 1 Torr by UVC irradiation using the 185 nm line (6 W) from a 25 W (254 nm + 185 nm light) low-pressure mercury lamp (Ebara Corp. Tokyo, Japan). UVC activation having a lower energy than the RF-plasma does not lead to cationic or anionic oxygen species but to atomic (O) and excited oxygen (O*) due to the UVC light at 185 nm [8].

2.2. Sputtering of TiO$_2$ on PE, X-ray fluorescence analysis, diffuse reflectance spectroscopy (DRS) and X-ray diffraction (XRD)

The TiO$_2$ was sputtered by direct current magnetron sputtering (DC) on PE in the presence of a low amount of O$_2$ [17]. Before sputtering the films, the residual pressure P_r was set to $P_r \leq 10^{-4}$ Pa. The substrate to target distance was 10 cm. The TiO$_2$ thin films were deposited in O$_2$ atmosphere from a 5 cm diameter Ti-target 99.99% pure (Kurt J. Lesker, East Sussex, UK). The current used on the Ti target was 280 mA (128 W). The Ti-content in the PE was evaluated by X-ray fluorescence (XRF) in a PANalytical PW2400 spectrometer.

The film thickness was determined with a profilometer Alphatest500, Tencor sputtering silicon wafers presenting a non-porous flat surface. Diffuse reflectance spectroscopy (DRS) of TiO$_2$ sputtered films was carried out a Perkin Elmer Lambda 900 UV–VIS-NIR spectrometer within the wavelength range of 200–800 nm. The crystalline structure of the PE-TiO$_2$ film was investigated by X-ray diffraction (XRD) and recorded on an X'Pert MPD PRO from PANalytical with an acquisition time of 2 min per degree.

2.3. X-ray photoelectron-spectroscopy (XPS), atomic force microscopy (AFM) and dynamic contact angle (DCA)

The X-ray photoelectron spectroscopy (XPS) of the loaded PE-TiO$_2$ samples (XPS) was determined using an AXIS NOVA photoelectron spectrometer (Kratos Analytical, Manchester, UK) provided for with monochromatic AlK$_\alpha$ ($h\nu$ = 1486.6 eV) anode. The electrostatic charge on the samples was compensated by means of the low-energy electron source working in combination with a magnetic immersion lens. Peak XPS signals were evaluated using sensitivity known factors [27,28]. The spectrum background was subtracted according to Shirley [29]. The XPS spectral peaks of TiO$_2$ were deconvoluted with from CasaXPS-Vision 2, Kratos Analytical UK.
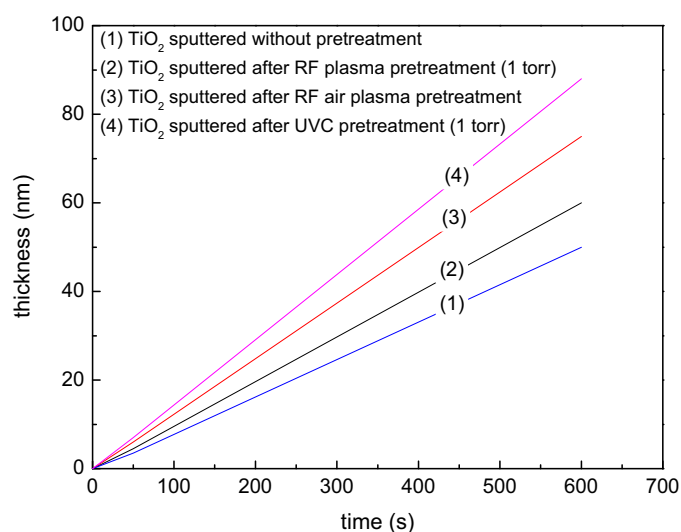

Fig. 1. Thickness calibration silicon wafers (1) no RF-pretreatment of PE, (2) PE pretreated with RF plasma for 15 min at 1 Torr, (3) PE pretreated with air by RF-plasma for 15 min and (4) PE pretreated with UVC for 20 min at 1 Torr.

The AFM image signals were acquired in contact mode using a PSIA Xe-100 AFM. Silicon nitride cantilevers were used with feedback set points around 1.0 nN. The measurements in the z-scanner were not influenced by the hysteresis in the z-scanner. The mean surface roughness (Rg) was calculated by Eq. (1)

$$R_a = \sqrt{\sum_{x,y}^{N} \frac{(Z_{x,y} - Z_{\text{average}})^2}{N^2}} \qquad (1)$$

R_a is the normalized standard deviation calculated from the local heights ($Z_{x,y}$) and the average height (Z_{average}) was determined over the x, y coordinates (N) on the AFM image.

The film hydrophilicity was determined by dynamic water droplet contact angle (CA) at different times for the TiO$_2$ sputtered samples by the sessile drop method on a DataPhysics OCA 35 unit. The irradiation source used was a Suntest solar light simulator (52 mW/cm^2).

2.4. Infrared spectroscopy (ATR-FTIR) and light irradiation source

FTIR spectra were measured in a Portmann Instruments AG spectrophotometer equipped with a Specac attachment (45° one pass diamond crystal). Spectra were taken by 256 scans with a resolution of 2 cm^{-1} in the range 900–4000 cm^{-1}. The position of the IR peaks was found by the second derivative of the spectra after Fourier deconvolution. The irradiation source was a Suntest solar light simulator (52 mW/cm^2).

3. Results and discussion

3.1. PE-TiO$_2$ layer thicknesses, TiO$_2$ loadings, DRS, rugosity and XRD

Fig. 1 shows the thickness of the TiO$_2$ layers sputtered on PE under different pretreatment conditions. Fig. 1; trace 3 shows the results of PE-pretreated with plasma in air at atmospheric pressure for 15 min and sputtered for 8 min. Vacuum is introduced in a sputtering magnetron chamber to decrease the collisions between the ions/electrons generated in the chamber. This leads to longer capture (diffusion) length of the metal–electron pairs generated in the chamber. This explains the difference in thickness as a function of sputtering time for the layers shown in Fig. 1; traces 2 and 3.

Table 1
X-ray fluorescence determination (XRF) analyses of TiO$_2$ on PE samples sputtered for different times with and without PE-pretreatment.

Sample	Surface TiO$_2$ wt %/wt PE
PE-TiO$_2$ (1 min), no pretreatment	0.009
PE-TiO$_2$ (3 min), no pretreatment	0.019
PE-TiO$_2$ (5 min), no pretreatment	0.031
PE-TiO$_2$ (8 min), no pretreatment	0.051
PE-TiO$_2$ (8 min), RF plasma pretreated under vacuum 15 min (1 Torr)	0.081
PE-TiO$_2$ (8 min), RF air plasma pretreated for 15 min	0.096
PE-TiO$_2$ (8 min), UVC pretreated for 20 min (1 Torr)	0.101

RF-plasma in the presence of O$_2$ (air) generates anions and cations (O$^-$, O$^+$), radicals, excited O* sates, molecular-ions and high-energy electrons in a system that is not in equilibrium. But UVC activation providing a lower energy input than the RF-plasma, does not lead to cationic or anionic oxygen species and only atomic (O) and excited oxygen (O*) species due to the applied 185 nm light. The radiant energy at 185 nm is below 241 nm (495 kJ/mol), the energy required for the reaction O$_2 \rightarrow$ 2O*. The absence of cationic or anionic oxygen leads to more uniform distribution in the activated sites on PE. This in turn to leads to more uniform TiO$_2$ layers [4–8]. This explains the larger thickness of TiO$_2$ film on the UVC pretreated PE compared to the RF-plasma pretreated sample in Fig. 1; trace 4.

Since one atomic layer contains ∼10^{15} atoms/cm^2 and is ∼0.2 nm thick [30,31], 60 nm thick layers contain ∼300 layers TiO$_2$. The Ti deposition rate was 2 × 10^{15} atoms/cm^2 s.

TiO$_2$ sputtering for 8 min samples pretreated by air plasma for 15 min led to the highest TiO$_2$ loading without affecting the PE color. The change of PE color has been reported as indicative of PE-degradation [32]. Ohtani [33] has reported PE degradation when TiO$_2$ nanoparticles were embedded in the PE but not for nanoparticles on the topmost PE layers.

Table 1 shows the surface atomic percentage concentration of TiO$_2$ as determined by XRF. The values in Table 1 show a higher TiO$_2$ loading for pretreated samples compared to non-pretreated samples. The sample pretreated in air for 15 min and then sputtered for 8 min (0.096% wt TiO$_2$/wt PE) lead to the fastest MB discoloration under simulated solar irradiation.

Fig. 2 presents the sample DRS spectra of sputtered for 8 min and pretreated by RF-plasma and UVC under different conditions PE-TiO$_2$ in Kubelka-Munk units as noted in the caption to Fig. 2. The absorption of the sample is plotted in Kubelka-Munk (KM) units. The rough UV–vis reflectance cannot be used directly to assess the absorption coefficient of the PE-TiO$_2$. Normally a weak dependence is assumed for the scattering coefficients on the wavelength. In Fig. 2; trace 2 the sample pretreated by RF for 15 min and sputtered for 8 min shows the fastest discoloration (Figs 7 and 8). This sample does not present the highest optical absorption in Fig. 2.

Fig. 3a shows the trend for higher Rg values as function of the TiO$_2$ loading and RF-pretreatment. The increase in rugosity (Rg) was observed to be more significant for pretreated samples compared to the non-pretreated samples due to the higher TiO$_2$ content presenting a higher TiO$_2$ BET area. Sample 3c shows that the fastest MB discoloration kinetics did not correspond to the Rg roughness of 11 nm. Rg values <16 nm (Fig. 3a), makes unlikely that the roughness variation between the samples will have any significant effect on the contact angle (CA) shown below in Fig. 4. Fig. 3 shows the trend for higher Rg values as function of the TiO$_2$ loading and RF-pretreatment.

Fig. 3b presents the XRD results of the PE-TiO$_2$ films. Fig. 3b shows the TiO$_2$ crystal phases on PE without pretreatment and
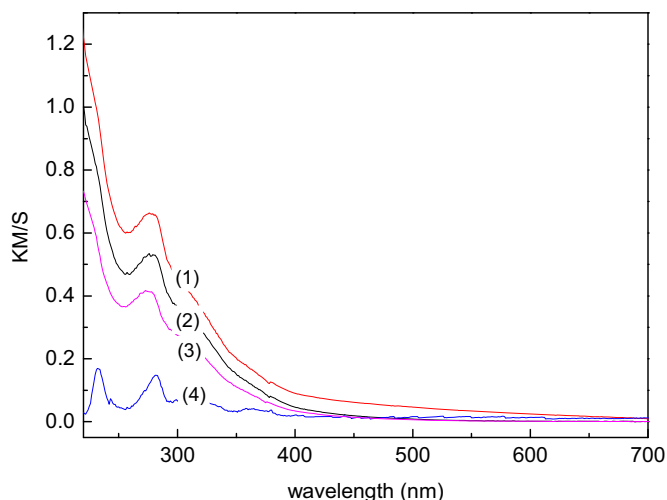

Fig. 2. DRS of the PE-TiO$_2$ sputtered (8 min) films: (1) pretreated with UVC for 15 min at 1 Torr, (2) pretreated with RF air plasma for 15 min, (3) pretreated with RF-plasma at 1 Torr for 15 min and (4) TiO$_2$ sputtered on PE for 1 min without pretreatment.

RF-plasma pretreated by XRD analysis. The result presented in Fig. 3 shows a high anatase (A) peak at θ = 21.5° for a PE-TiO$_2$ samples sputtered for 8 min with and without RF-plasma pretreatment. Fig. 3b shows also the XRD peaks of rutile (R) produced at temperatures ≤130 °C available in the DC-magnetron chamber. Generally the appearance of rutile phase in TiO$_2$ colloidal suspensions is not possible below 500 °C as is a function of the length of the thermal treatment. The generation of rutile at low temperatures is due the structure forming function of the PE film on the TiO$_2$ and was previously reported for polyamide textiles [9,34,35]. The intensity of the anatase peaks shown in Fig. 3b became more intense as a function of the sputtering time as expected for samples pretreated or not by RF-plasma.

3.2. Contact angle (CA) and reversible photo-switching

Fig. 4a shows the reduction in the contact angle of PE-TiO$_2$ as a function of the irradiation time due to the increase in the hydrophilic nature of the PE-TiO$_2$ film under light [36–38]. PE-TiO$_2$ sputtered for 8 min present a contact angle of 121° at time zero. Fig. 4b shows that the recovery of the PE-TiO$_2$ hydrophilic surface to the initial hydrophobicity proceeds within 24 h in the dark. The hydrophilicity of the PE-TiO$_2$ under irradiation was attained within 60 min. This time is below 2 h, the time necessary to completely discolor MB as shown Fig. 7a.

According to Young's theory, the "cos θ" of a liquid droplet on a solid surface is a function of the interfacial energy between the solid and the liquid. The contact angle (CA) conventionally measures the angle where the liquid meets the solid quantifying the wettability of a solid surface via the Young equation. The Young equation involves solid–vapor, liquid–vapor and solid–liquid interfacial energies. The solid–vapor interfacial energy is labeled γSG, the solid–liquid interfacial energy γSL and the liquid-vapor interfacial energy i.e. the surface tension by γLG. The equilibrium contact angle θC is determined from these quantities by Young's equation:

$$0 = \gamma SG - \gamma SL - \gamma LG \cos \theta C \tag{2}$$

In Eq. (2), γ is the surface free energy and $t = \infty$ corresponds to the interfacial energy of the hydrophobic surface before irradiation.

Fig. 5a illustrates the kinetics for the photo-induced hydrophilicity. Fig. 5b shows the back reaction kinetics to the initial hydrophobic surface as function of "cos θ" [39]. The rate of the hydrophobic to hydrophilic conversion and for the reverse
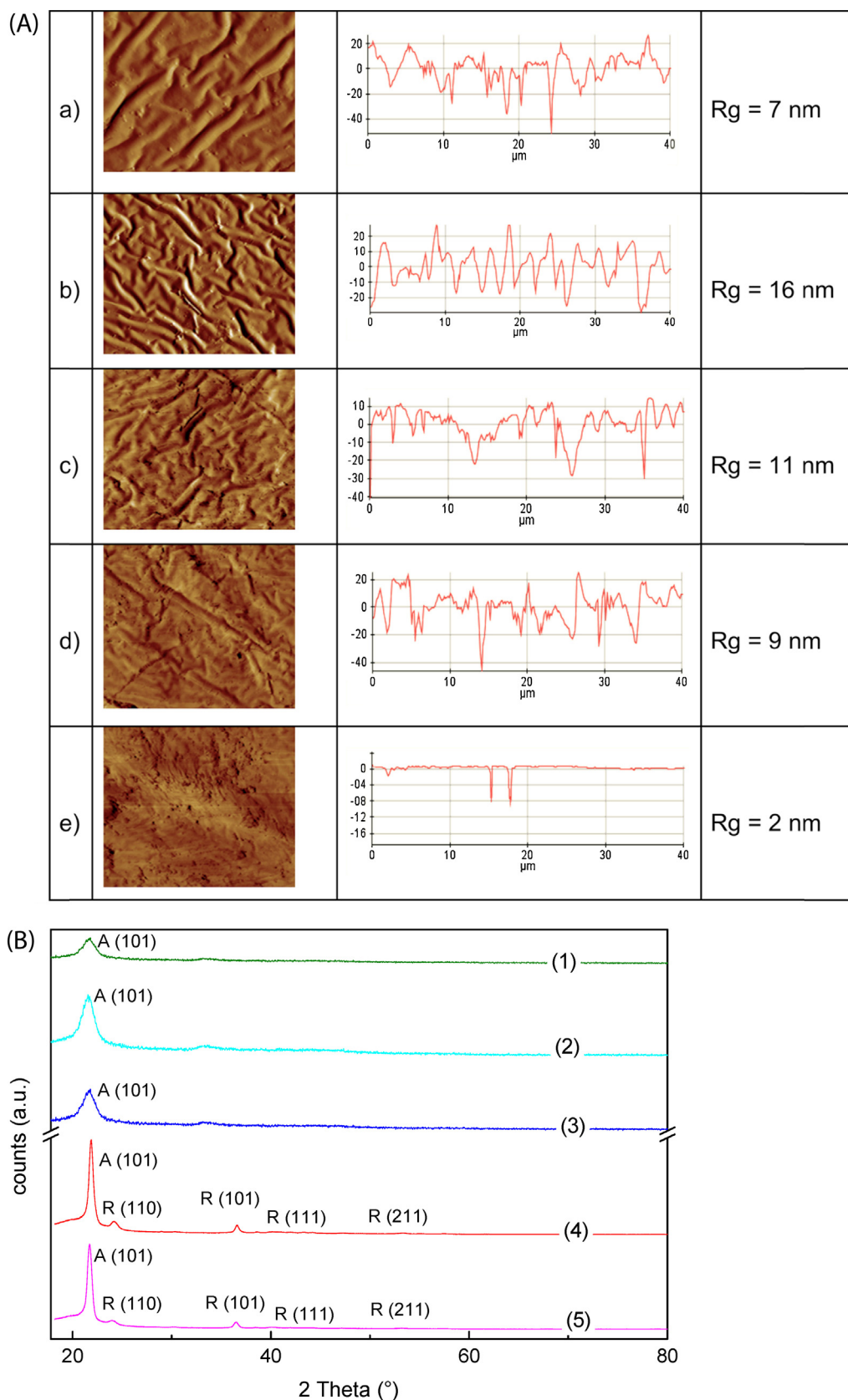
Fig. 3. (A) AFM topography of PE-TiO$_2$ samples sputtered for 8 min: (a) TiO$_2$-PE, no pretreatment, (b) PE-TiO$_2$ RF plasma pretreated at 1 Torr for 15 min, (c) PE-TiO$_2$ RF air plasma pretreated for 15 min, (d) PE-TiO$_2$ UVC pretreated for 20 min in air, (e) PE-TiO$_2$ RF pretreated for 15 min and sputtered for 1 min. (B) Crystal phases of PE-TiO$_2$ sputtered: (1) pretreated with RF-air plasma for 15 min, sputtered for 1 min (2), no pretreatment sputtered for 5 min, (3) no pretreatment, sputtered for 1 min (4) pretreated with RF-air plasma for 15 min, sputtered for 8 min and finally (5) sputtered for 8 min without pretreatment.

A a) 121°   b) 108°   c) 89°   d) 44°   e) <5°

B a) 37°   b) 81°   c) 106°   d) 118°
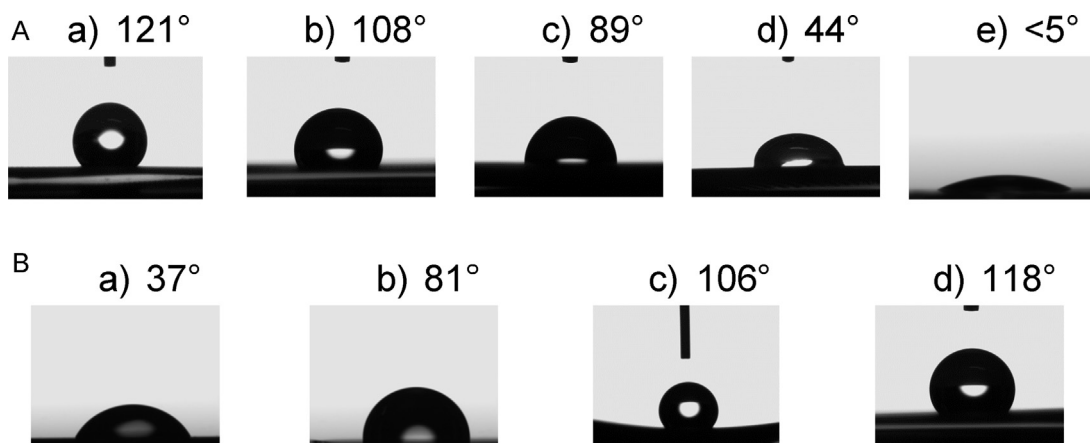
Fig. 4. (A) Photo-induced super-hydrophilicity for a PE-TiO$_2$ sample RF-treated 15 min and sputtered 8 min followed by water droplet contact angle induced by light i at times: (a) $t = 0$ min, (b) 15 min, (c) 30 min, (d) 45 min and (e) 60 min. (B) Restoration of the hydrophobicity in the dark for the sample described in Fig. 5a after: (a) 6 h, (b) 12 h, (c) 18 h and (d) 24 h.

reaction were: 0.277 min^{-1} and 8.71×10^{-3} min^{-1} respectively (from Fig. 5a and b).

3.3. XPS analyses of PE-TiO$_2$ film surfaces

Fig. 6a–c shows the PE-TiO$_2$ envelope and the deconvoluted XPS band components before and after pretreatment. The peaks of the Ti—O, Ti—OH and O—C signals for non-pretreated PE-TiO$_2$ samples are shown in Fig. 6a. Fig. 6b presents a PE-TiO$_2$ sample pretreated in air plasma for 15 min showing a significant increase in the Ti—O peak with respect to the Ti—O peak found in Fig. 6a. The Ti—O and Ti—OH species in the deconvoluted peaks are shown in Fig. 6a–c and were estimated by introducing the sensitivity factor for oxygen [27]. The Ti—OH bands on PE-TiO$_2$ detected by XPS are shown in Fig. 6a–c at 532.4 eV, 532.7 eV and 532.9 eV.

In Fig. 6a–c the TiO$_2$ particle on the PE seems to be strongly hydroxylated, as reflected in the OH-surface component observed at 532.4 eV in Fig. 6a. Dhananjeyan et al. [40] presented evidence for the signal of a TiOH copolymer. When compared with the hydroxylation of the TiO$_2$ Degussa powders with a signal for the O 1s at 529.5 eV. The TiOH copolymer signal was very high compared with the ones we found for the oxygen O 1s TiO$_2$ powder at 529.5 eV.

Table 2
Surface percentage atomic concentration of PE-TiO$_2$ sputtered for 8 min, before MB discoloration.

Sample	C	O	Ti	N
No pretreated PE	52.37	30	6.17	0.00
RF air plasma	55.14	33.27	8.82	0.07
RF plasma	53.58	31.84	7.44	0.09
UVC	54.01	33.11	7.62	0.11

A redox process during RF-plasma pretreatment takes place during the sample pretreatment since a shift ≥ 0.2 eV was observed for samples pretreated with respect to the non-pretreated sample in Fig. 6a [40]. Fig. 6c shows the XPS signals for an RF-pretreated sample for 15 min and 1 Torr. A redox reaction for the Ti—O takes place, since this peak shifts position respect to the peak for the PE-TiO$_2$ sample without pretreatment at 532.4 eV (Fig. 6a).

Fig. 6d shows that no Ti—OH signals could be detected for an UVC PE-TiO$_2$ sample pretreated for 20 min. The disappearance of the Ti—OH peak was due to a thermal effect caused by the temperature increase due to UVC light irradiation. This shows that the PE-TiO$_2$ does not contain chemisorbed water [28,40].

Table 2 shows the surface percentage atomic concentration of PE-TiO$_2$ sputtered for 8 min, before MB discoloration. During
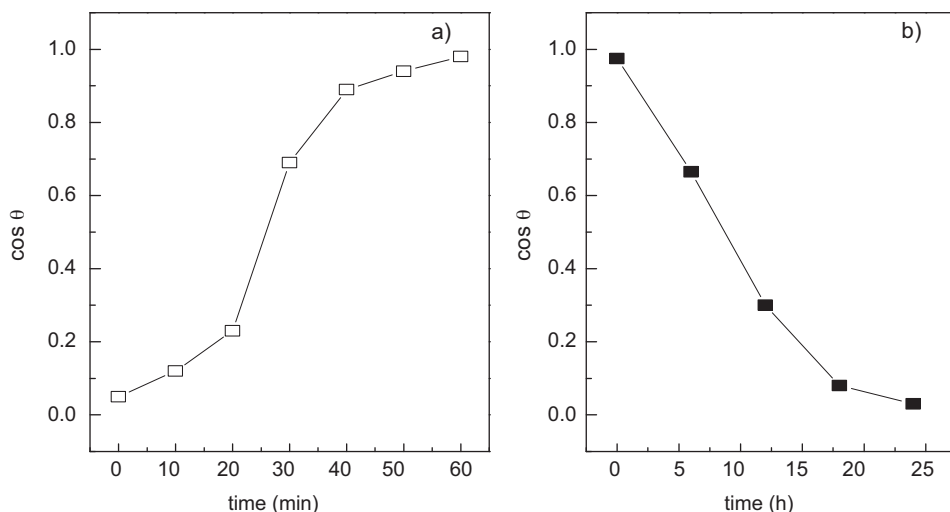
Fig. 5. (a) Kinetics of the hydrophobic–hydrophilic transformation of PE-TiO$_2$ RF-plasma PE-TiO$_2$ air pretreated for 15 min and sputtered for 8 min under solar simulated light and (b) kinetics of the reverse reaction in the dark re-establishing the initial PE-TiO$_2$ film hydrophobicity.
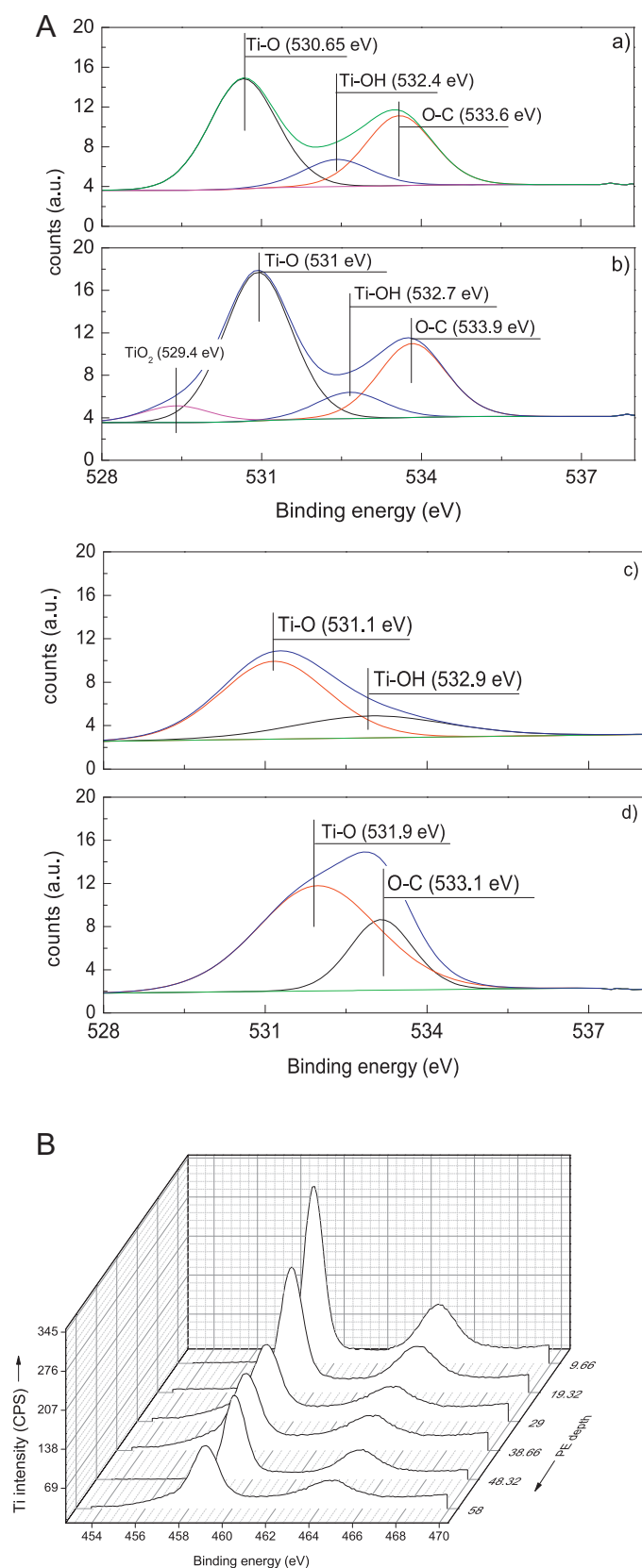
Fig. 6. (A) O 1s deconvolution of PE-TiO₂ XPS spectral peaks: (a) no pretreatment, (b) after RF air plasma pretreatment during 15 min, (c) RF-plasma pretreatment for 15 min (1 Torr) and (d) UVC pretreatment for 20 min (1 Torr). (B) Tri-dimensional plot showing the Ti-penetration into the RF-plasma PE-TiO₂ air pretreated for 15 min and sputtered for 8 min: (a) *x*-axis, the Ti 2p doublet BE, (b) *y*-axis, the relative intensity of the Ti-peaks and (c) *z*-axis, the depth profile of an Ar-etched PE-TiO2 as a function of the distance to the PE surface in nm.
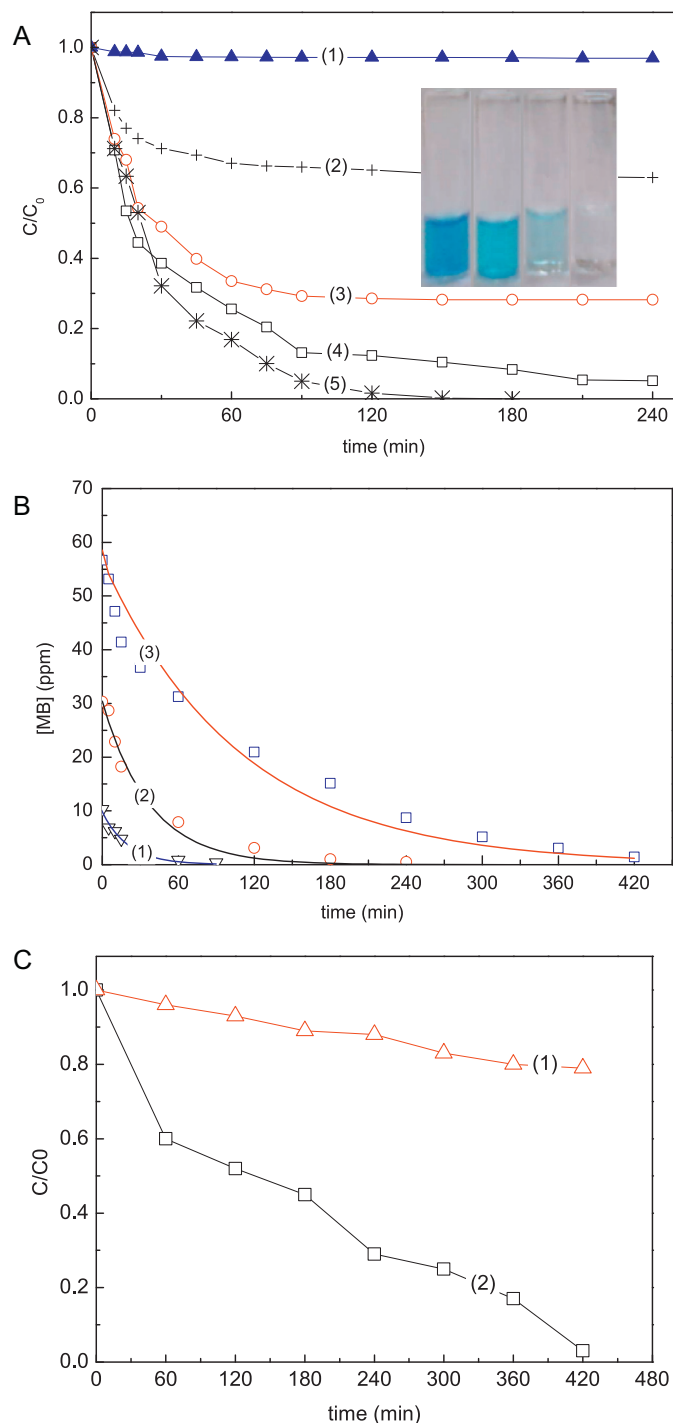
Fig. 7. (A) Solar simulated light induced discoloration of MB solutions followed at 664 nm by: (1) PE alone, (2) PE-TiO₂ sputtered for 5 min, (3) PE-TiO₂ sputtered for 8 min, (4) PE-TiO₂ sputtered for 15 min, no pretreatment (5) PE-TiO₂ sputtered for 8 min RF plasma pretreated for 15 min. The insert shows the discoloration of an MB 30 ppm solution using sample 5 as a function of irradiation time 15, 30, 60 and 120 min. (B) MB stain discoloration kinetics under solar simulated light on PE-TiO₂ sputtered samples for 8 min and RF plasma pretreated for 15 min. The MB stains applied on PE contained: (1) 100 ml/cm² (10 ppm) (2) 100 ml/cm² (30 ppm) and (3) 100 microliters/cm² (60 ppm). (C) Discoloration by a low intensity Philips TLD 18 W BLB UV light (2.7 mW/cm²) of a MB stain MB 100 ml (30 ppm) by: (1) PE-TiO₂ sputtered sample for 8 min and (2) PE-TiO₂ sputtered sample for 8 min and RF plasma pretreated (15 min).

the RF-plasma and UVC pretreatment the air containing CO_2 is treated/irradiated in the respective chambers. By XPS as shown in Table 2 the signal increases on PE pretreated samples respect to non-pretreated samples due to the adventitious hydrocarbons being adsorbed from the ambient air in the chamber on the sample surface.

Different PE pretreatment times gives rise to a different Ti—O—C boundary layer between PE and TiO_2. This promotes a different reactivity between MB and the PE-TiO_2 samples at TiO_2 thicknesses [20,34,35,41].

The etching by XPS Ar-ions bombardment of PE-TiO_2 is shown in the tridimensional plot in Fig. 6b, showing the Ti-penetration depth into for an RF-plasma pretreated PE-TiO_2 sample sputtered for 8 min. The Ti 2p peaks show the continuous decrease of Ti from the PE surface down to 58 nm. This is equivalent to ~290 layers since each atomic layer is estimated to be ~0.2 nm thick [31].

3.4. MB discoloration kinetics under simulated solar and UV light

Fig. 7a shows the discoloration of MB solutions by transparent PE-TiO_2 films under simulated solar light (52 mW/cm^2). A higher TiO_2 loading led to faster discoloration kinetics. The PE-TiO_2 film RF-air plasma pretreated for 15 min and sputtered for 8 min shown in trace 5 discolors the MB solution within 120 min (see far right transparent solution in the insert in Fig. 7).

Fig. 7a; traces 2,3 present a leveling-off of the discoloration at longer irradiation times was observed. Table 1 shows the TiO_2 content of the samples used to obtain the discoloration results reported in Figs. 2 and 3. The loadings of 0.031% and 0.051% seem not to be enough to generate sufficient highly oxidative radicals on the TiO_2 surface compared to the more heavily TiO_2 loaded TiO_2 samples reported in Fig. 7; traces 4 and 5.
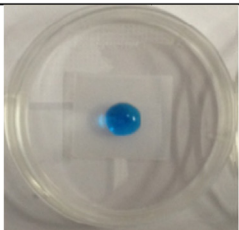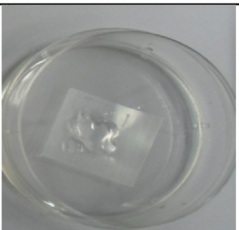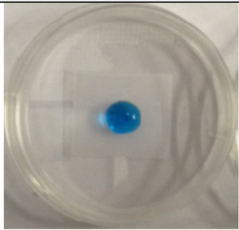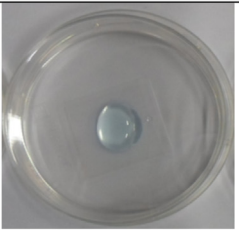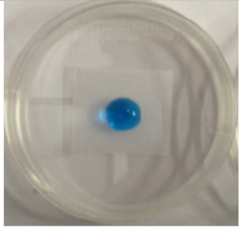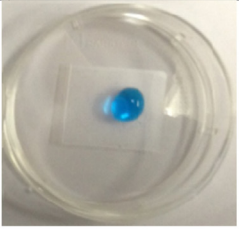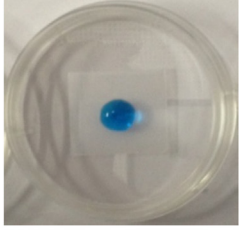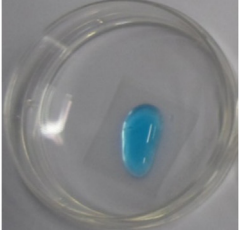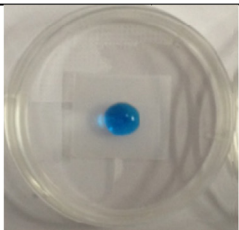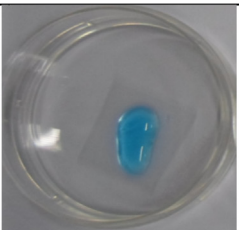
Irradiation	Initial state	Final state	Removal percentage
Solar simulated light UV cut-off 290 nm, (100 mW/cm^2)			98%
Solar simulated light, UV cut-off 310 nm (100 mW/cm^2)			92%
Solar simulated light, UV cut-off 400 nm (100 mW/cm^2)			5%
Solar simulated light UV cut-off 310 nm (52 mW/cm^2)			8%
Low intensity actinic/visible light (10.0 mW/cm^2)			7%

Fig. 8. Visual perception of the MB discoloration on PE-TiO_2 sputtered for 8 min and pretreated with RF-plasma for 15 min under different light sources and light intensities.
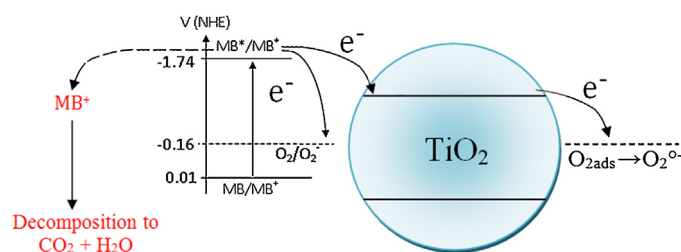
Scheme 1. in p12: Electron injection mechanism of MB into TiO_2 under sunlight irradiation.

Scheme 1 shows the formation of an MB^* excited state under light irradiation leading to a short lived unstable cation that subsequently decomposes and concomitantly: (a) injects an electron on TiO_2. This electron is transferred to the adsorbed O_2 adsorbed on the TiO_2 surface leading to $O_2^{\circ-}$ and other highly oxidative radicals or (b) reacts with the O_2 present in the solution.

The left hand side in Scheme 1 shows the energy levels of the MB ground state (g.s.) and the excited state MB^* and the e^- injection pathways. A discussion on the mechanism, thermodynamics and the probability of the MB^* deactivation pathway in relation to the reaction of $MB^* +$ solution O_2 is addressed below.

The low energy edge of MB has been reported at 720 nm or 1.75 eV [23]. The photosensitization by MB of $PE-TiO_2$ in Scheme 1 leads to a quenching MB^* with concomitant charge transfer and the formation of MB^+ as noted in Eq. (3)

$$MB + PE\text{-}TiO_2 + solarlight \rightarrow [MB*\dots TiO_2]PE \rightarrow MB^+$$

$$+ [PE\text{-}TiO_2 + e^-] \qquad (3)$$
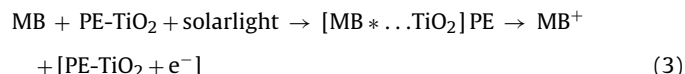
On thermodynamic grounds, the charge transfer from MB^* to TiO_2 is possible since the potential of the oxidative half-cell MB/MB^+ is ~ 0.01 V at pH7 (NHE) [23,45]. Because the low-energy absorption edge of MB located at 720 nm or 1.75 eV, the excited-state standard potential of MB can be estimated from the energy-gap ΔG^0 [34,35]. The gap ΔE° between the ground state and the excited state of MB is

$$\Delta E^\circ \ (MB^+/MB^*)(V) = E^\circ(MB^+/MB) - \Delta G^\circ(MB^*/MB) \qquad (4)$$

Inserting the values in Eq. (4) as (0.01−1.75), a value of −1.74 V (NHE) is found for the excited state potential of MB. Since the potential of the couple O_2/O_2- is −0.16 V (NHE) the charge transfer from MB to O_2 seems to be thermodynamically feasible. The fast discoloration kinetics is driven by the high potential-difference between MB/MB^+ and O_2/O_2^- levels (Scheme 1). The MB^* excited state in Scheme 1 involves a short lived singlet with a lifetime of 358 ps, followed by intersystem crossing to the lower lying triplet with a lifetime 4.5 ms and a quantum yield of 0.52 [42–45].

If t is the lifetime of the MB triplet (4.5 ms), k the diffusion control rate for the reaction MB with O_2 in aqueous solution $(\sim 9.6\,10^9\,M-1\,s-1)$ and the oxygen concentration in the MB solution $[O_2] \approx 0.5 \times 10-3$ M, the probability P_1 for the triplet MB deactivation $P_1 = (t^{-1})/[(t^{-1} + k\,[O_2] \approx 0.04$. The probability P_2 of reaction between $MB^* + O_2 \rightarrow MB^+ + O_2o^-$ leading to MB^+ cation formation can be estimated from the relation $k\,[O_2]/[(t^{-1}) + k[O_2]] \approx 0.53$. The mechanism of the light induced discoloration of MB on TiO_2 has been reported and will not be discussed further [21–26,45].

Fig. 7b shows that the discoloration kinetics of MB slows down with an increasing amount of MB. The apparent rate for each MB concentration was estimated. The rates were very similar with values between 0.36 and 0.4 s^{-1}.

Fig. 7c shows the MB discoloration by: (1) $PE-TiO_2$ sputtered sample for 8 min and (2) $PE-TiO_2$ sputtered sample for 8 min and
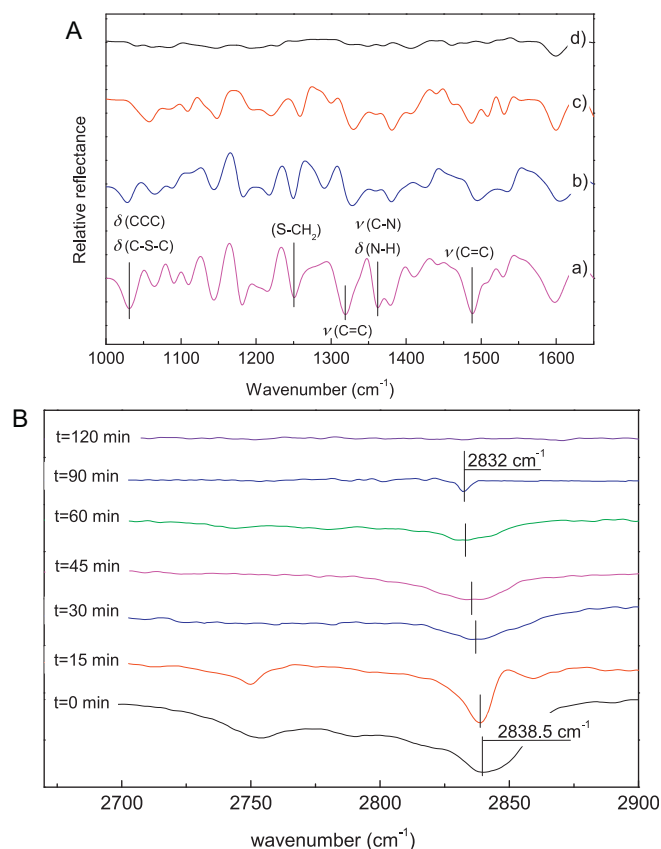

Fig. 9. (A) Solar simulated light induced MB degradation on RF-plasma pretreated $PE-TiO_2$ samples for 15 min and sputtered for 8 min followed by ATR-FTIR spectroscopy: (a) time zero, (b) time 30 min, (c) time 60 min and (d) time 120 m. (B) Change in the amplitude and position of the MB $\nu_s(-CH_2)$ vibrational peaks as a function of solar simulated irradiation time on RF-plasma pretreated $PE-TiO_2$ samples for 15 min and sputtered afterwards for 8 min.

RF plasma pretreated (15 min). This readily shows the significant effect of the pretreatment increasing the loading of TiO_2 on PE with beneficial effects on the MB degradation efficiency.

Fig. 8 presents the visual perception of the discoloration by $PE-TiO_2$ of MB on PE pretreated by RF-plasma for 15 min when irradiated with different light sources/intensities. The UV-component is seen to play a crucial role in the removal percentage of MB on the $PE-TiO_2$ samples. MB discoloration in Fig. 8 is shown to be highly dependent on the lamp intensity and wavelength.

During the discoloration of MB $PE-TiO_2$ a shift of about 2.5 nm was observed for the 664 nm peak into the blue region reaching a plateau after 120 min. This effect could be attributed to the MB electronic delocalization modifying the extinction coefficient of MB on $PE-TiO_2$ [45]. A hypsochromic shift is not probable, since any blue shift may be due to the superposition of the spectra of different intermediated produced during MB discoloration.

3.5. FTIR-ATR spectroscopy during MB discoloration on $PE-TiO_2$

FTIR spectroscopy was used to monitor the MB degradation under solar simulated light. Fig. 9a shows at time zero the characteristic vibrations of the conjugated bonds in the MB aromatic ring (C=C), as well as the IR peaks assigned to (C−N), (S−CH) and (C−S−C).

The signals in Fig. 9a were sensitive enough to follow the IR-spectral shifts and changes of amplitude during MB discoloration on $PE-TiO_2$ under simulated sunlight. Fig. 9b shows the decrease of the C−N ART-IR peak reported in trace a at time zero and at

the end of the MB discoloration (120 min) as shown in trace d. The lysis of terminal N—C(benzene ring) requires more energy compared to the energy to brake the N≡C(benzene ring) double bond (see in Ref. [46,47] Fig. 6). Fig. 9a also shows the vibrational bands of the less stable amines (N—H) decreasing rapidly compared to: (a) the (—CH$_2$) bands at around 2838 cm^{-1} and (b) the aromatic (C=C) around 1487 cm^{-1}.[46]

The methylene (—CH$_2$) stretching vibration in the range 2700–2900 cm^{-1} is shown in Fig. 9b. The ATR-IR signals being much bigger than the signals observed for C—N at 1252 cm^{-1} made it possible to follow in the time scale the reduction of amplitude and peak changes for the (—CH$_2$) stretching vibration as reported next in Fig. 9b. Fig. 9b shows a discontinuous shift of the methylene symmetric stretching vibration v_s(—CH$_2$) from 2838 cm^{-1} at time zero up to 2832 cm^{-1} within 120 min when the signal vanishes [48,49]. The shift is due to an increase in the vibrational stretching up to 120 min when bond scission was attained. The disappearance of the stretching vibrations of the aromatic (C=C) at 1487 cm^{-1} within 120 min irradiation was also observed (data not shown).

4. Conclusions

- This study presents the first report for MB discoloration on transparent non-scattering PE-TiO$_2$ sputtered films.
- The MB discoloration on RF-plasma pretreated PE leads to an accelerated kinetics compared with non-pretreated PE.
- Evidence is presented for the shift in functional groups stretching vibrations for MB under light irradiation on PE-TiO$_2$ films
- The probability for the MB* deactivation was estimated and was observed to be lower compared to the probability for the reaction between MB*+O$_2$
- Evidence for the IFCT occurring between MB and TiO$_2$ is presented based on the position of the band potential energies. A mechanism of reaction is suggested between MB and TiO$_2$ under solar simulated light.

Acknowledgments

References

[1] W. Tung, W. Daoud, J. Mater. Chem. 21 (2011) 7858–7869.
[2] J. Kiwi, C. Pulgarin, in: W. Daoud (Ed.), Self-cleaning Materials and Surfaces, Woodhead Pub. Co., UK, 2013, pp. 205–224 (Chapter 7).
[3] K. Meilert, D. Laub, J. Kiwi, J. Mol. Catal. A. 237 (2005) 101–108.
[4] A. Bozzi, T. Yuranova, I. Guasaquillo, D. Laub, J. Kiwi, J. Photochem. Photobiol. A 174 (2005) 156–164.
[5] T. Yuranova, R. Mosteo, J. Bandara, D. Laub, J. Kiwi, J. Mol. Catal. A 244 (2006) 160–167.
[6] A. Bozzi, T. Yuranova, J. Kiwi, J. Photochem. Photobiol. A 172 (2005) 27–34.
[7] M.I. Mejia, J.M. Marin, G. Restrepo, C. Pulgarin, E. Mielczarski, J. Mielczarski, Y. Arroyo, J.-C. Lavanchy, J. Kiwi, Appl. Catal. B 91 (2009) 481–488.
[8] M.I. Mejia, J.M. Marin, G. Restrepo, C. Pulgarin, E. Mielczarski, J. Mielczarski, J. Kiwi, ACS Appl. Mater. Interface 1 (2009) 2190–2198.
[9] K. Qi, W. Daoud, J. Xin, C. Mark, W. Tang, W. Cheung, J. Mater. Chem. 16 (2006) 4567–4574.
[10] S. Afzai, W. Daoud, S. Langford, Appl. Surf. Sci. 75 (2013) 36–42.
[11] D. Mihailovic, Z. Saponjic, M. Radoicic, S. Lazovic, C.J. Baily, P. Jovancic, J. Nedeljkovic, M. Radetic, Cellulose 18 (2011) 811–825.
[12] J. Kasanen, M. Suvanto, T.T. Pakkanen, J. Appl. Polym. Sci. 111 (2009) 2597–2602.
[13] L. Zhang, R. Dillert, D. Bahnemann, M. Vormoor, Energy Environ. Sci. 5 (2012) 7491–7507.
[14] T. Yuranova, G. Rincon, A. Bozzi, S. Parra, C. Pulgarin, P. Albers, J. Kiwi, J. Photochem. Photobiol. A 161 (2003) 27–34.
[15] S. Rtimi, C. Pulgarin, R. Sanjines, J. Kiwi, RSC Adv. 3 (2013) 16345–16349.
[16] C.M. Chan, T. Ko, H. Hiroaka, Surf. Sci. Rep. 24 (1996) 1–54.
[17] O. Baghriche, S. Rtimi, R. Sanjines, C. Pulgarin, J. Kiwi, J. Photochem. Photobiol. A 251 (2013) 50–56.
[18] A. Mills, S. Lee, J. Photochem. Photobiol. C. 152 (2001) 33–247.
[19] K. Sarakinos, J. Alami, D. Konstantinidis, Surf. Coat. Technol. 204 (2010) 1661–1684.
[20] H. Foster, I. Ditta, S. Varghese, A. Steele, Appl. Microbiol. Biotechnol. 90 (2011) 1847–1868.
[21] X. Qiu, M. Miyaguchi, K. Sunada, M. Minoshima, M. Liu, Y. Lu, D. Li, Y. Shimodaira, Y. Hosogi, Y. Kuroda, K. Hashimoto, ACS Nano 6 (2012) 1609–1618.
[22] A. Mills, J. Wang, J. Photochem. Photobiol. A 127 (1999) 123–134.
[23] A. Mills, Appl. Catal. B 128 (2012) 144–149.
[24] A. Mills, D. Hazafy, J. Parkinson, T. Tuttle, M. Hitchings, Dyes Pigments 88 (2011) 149–155.
[25] O. Impert, A. Katafias, P. Kita, A. Mills, A. Pietkewicz, G. Wrzeszcz, Dalton Trans. (2003) 348–353.
[26] A. Houas, H. Lachheb, M. Ksibi, E. Elalui, C. Guillard, J.-M. Herrmann, Appl. Catal. B 31 (2001) 145–157.
[27] C.D. Wagner, E.L. Davis, G.E. Müllenberg (Eds.), Perkin-Elmer Corporation Physical Electronics Division, Handbook of X-Ray Photoelectron Spectroscopy, Mn, USA, 1979.
[28] J. Nogier, M. Delamar, P. Ruiz, P. Albers, J. Kiwi, Catal. Today 20 (1994) 109–123.
[29] D.A. Shirley, Phys. Rev. B 5 (1972) 4709–4714.
[30] A. Ehiasarian, J. Anderson, A. Anders, J. Phys. Appl. Phys. 43 (2010) 275204.
[31] J. Mathews, Epitaxial Growth Part B, IBM Thomas Watson Research Center, Academic Press, New York, 1975, pp. 382–436.
[32] K. Tenakone, C. Tilikaratne, I. Kottegoda, J. Photochem. Photobiol. A 87 (1995) 177–183.
[33] B. Ohtani, S. Adzuma, S. Nishimoto, T. Kayiga, Polym. Degrad. Stabil. 35 (1992) 53–60.
[34] A. Fujishima, X. Zhang, A. Tryk, A. Donald, Surf. Sci. Rep. 63 (2008) 515–582.
[35] M. Lazar, W. Daoud, RSC Adv. 3 (2013) 4130–4140.
[36] R. Fürstner, W. Barthlott, C. Neinhuis, P. Walzel, Langmuir 21 (2005) 956–961.
[37] R. Wang, K. Hashimoto, A. Fujishima, A. Chikuni, M. Kojima, E. Kitamura, A. Shimohigishi, M. Watanabe, Nature 388 (1997) 431–436.
[38] N. Sakai, A. Fujishima, T. Watanabe, K. Hashimoto, J. Phys. Chem. B 105 (2001) 3023–3028.
[39] E.P. Ivanova, V. Truong, J.Y. Wang, C. Berndt, R. Jones, I. Yusuf, I. Peake, H. Schmidt, C. Fluke, D. Barnes, R. Crawford, Langmuir 26 (2009) 1973–1982, and references therein.
[40] M. Dhananjeyan, E. Mielczarski, K. Thampi, Ph. Buffat, M. Bensimon, A. Kulik, J. Mielczarski, J. Kiwi, J. Phys. Chem. B 105 (2001) 12046–12055.
[41] A. Harmer, E. Farneth, Q. Sun, J. Am. Chem. Soc. 118 (1996) 7708–7716.
[42] S. Kumar, L. Devi, J. Phys. Chem. A 115 (2011) 13211–13241.
[43] P.V. Kamat, Chem. Rev. 93 (2011) 267–300.
[44] Y. Gak, V. Nadtochenko, J. Kiwi, J. Photochem. Photobiol. A 116 (1998) 57–62.
[45] S.L. Murov, I. Carmichael, G.L. Hug, Handbook of Photochemistry, 2nd ed., Marcel Dekker, New York, 1993.
[46] V. Nadtochenko, A. Rincon, S. Stanka, J. Kiwi, J. Photochem. Photobiol. A (169) (2005) 131–137.
[47] G. Starukh, S. Toscani, S. Boursicot, L. Spahnel, Z. Phys. Chem. 221 (2007) 349–360.
[48] D. Naumann, C. Schultz, A. Sabich, M. Kasrowsky, H. Labishinsi, J. Mol. Struct. 214 (1989) 213–246.
[49] J. Kiwi, V. Nadtochenko, J. Phys. Chem. B 108 (2004) 17675–17684.